Regenerative Therapy 26 (2024) 620–634

Contents lists available at ScienceDirect

Regenerative Therapy

journal homepage: http://www.elsevier.com/locate/reth

Original Article

Novel fabrication of anti-VEGF drug ranibizumab loaded PLGA/PLA co-polymeric nanomicelles for long-acting intraocular delivery in the treatment of age-related macular degeneration therapy

Jin-feng Xu [1], Yan-ping Wang [1], Xiao-hua Liu*

Department of Ophthalmology, Dongying People's Hospital, Dongying 257001, China

ARTICLE INFO

Article history:
Received 8 May 2024
Received in revised form
6 June 2024
Accepted 27 June 2024

Keywords:
Ranibizumab
Copolymer
Nanomicelles
Retinal pigment epithelial cells
Cytotoxicity
Macular degeneration

ABSTRACTS

Age associated macular degeneration is the 3rd primary cause of blind fundus diseases globally. A reliable and long-lasting method of intraocular drug delivery is still needed. Herein, this study was aim to develop the novel fabrication of ranibizumab loaded co-polymeric nanomicelles (Rabz-CP-NMs) for AMD. The CMC of co-polymeric nanomicelles was determined to be low, at 6.2 μg/ml. The ring copolymerization method was employed to fabricate the NMs and characterize via FTIR, XRD, TEM, DLS and Zeta potential. Rabz-CP-NMs was spherical shape with 10–50 nm in size. Stable and prolonged drug release was achieved with the Rabz from CP-NMs at 48 h. D407 and ARPE19 ocular cell lines showed dose-dependent cell viability with Rabz-CP-NMs. The Rabz-CP-NMs also had less toxicity, higher uptake, lower cell death and prolonged VEGF-A inhibition, as shown by cytoviability assay. Thus, Rabz-CP-NMs were safe for ocular use, suggesting that could be used to improve intraocular AMD treatment.

1. Introduction

The primary cause of impairment in the older population in developed nations is age-associated macular degeneration (AMD), which is characterized by a gradual loss of visual acuity over time [1]. A future public health concern and economic burden, AMD is predicted to grow in number of people as life expectancy increases. Consequently, various therapeutic approaches for treating AMD are in development. Choroidal neovascularization, angiogenesis under and/or through the retinal pigment epithelium, is characteristic of the wet type of AMD, also known as the exudative form. One potential treatment for AMD is the blocking of VEGF, a crucial molecule involved in angiogenesis [2,3].

Nowadays, the primary approach to treating neovascular ophthalmopathy is by inhibiting VEGF activity. In most cases, anti-VEGF intravitreal injections can enhance visual results by inhibiting retinal neovascularization and vascular leakage, according to several surveys [4–6].

Several therapeutic techniques have been developed to lessen the impact of fundus neovascular disease on public health. These include vitrectomy, intravitreal steroid injection, anti-VEGF therapy, and pan retinal photocoagulation [7–9]. To attain an effective concentration of anti-VEGF medication in the eye, intravitreal injection is required once monthly [10]. However, this solution can somewhat block the continued production of retinal neovascularization. Patients bear a disproportionate share of the financial and emotional costs associated with intraocular injections, and the risk of ocular and systemic disorders increases dramatically as the number of injections increases [11,12]. Furthermore, with prolonged and repeated treatment, several patients demonstrated photoreceptor degradation and insensitivity to anti-VEGF medications [13]. The pharmaceutical industry has developed stronger, slowly-dissolving drugs with the goal of releasing tiny doses of these drugs into organs and tissues over a long period of time [14]. Research into controlled release methods to increase the duration of anti-VEGF drug effect in the eye is ongoing in the scientific community. To reduce the frequency of intravitreal injections while yet achieving continuous release and

* Corresponding author. NO.317, South 1st Road, Dongying 257001, China.
E-mail address: Xiao-hua2Liu@hotmail.com (X.-h. Liu).

Peer review under responsibility of the Japanese Society for Regenerative Medicine.

[1] Contribute equally to this study.

https://doi.org/10.1016/j.reth.2024.06.019

significant therapeutic effects, anti-VEGF medicines can be encapsulated in sustained-release polymers.

Ranibizumab (Rabz), the Fab fragment of a human derived mAbs (48 kDa; Novartis, Switzerland) has an affinity for all isotypes of VEGF-A and blocks its biological action. Research on the efficacy of Rabz has been extensively studied in clinical studies, such as MARINA (ranibizumab alone at various dosages) [15], ANCHOR (ranibizumab vs. photodynamic rehab with verteporfin) [16,17], and PIER (optimization of drug interval) [18,19]. As a first-line treatment for AMD, ranibizumab has also received broad approval for the control of macular edema caused by retinal veins blockage [20,21] and diabetic macular edema [22]. Therefore, in order to solve this problem, it is necessary to seek the administration of a regulated drug delivery system.

According to the literature we study, nanotechnology improves retinal medication delivery by increasing drug solubility, bioavailability, penetration, absorption area, and injection frequency. For effective ocular drug delivery, nanoparticle form, size, substance, and surface must be considered. It should be large enough to minimize rapid leaking into blood vessels but small enough to inject or penetrate retinal cellular barriers [23,24]. Note that nanoparticles with comparable sizes but varied surface qualities may have different distributions inside the eye [25], which might help optimize their physical-chemical properties for retinal medication delivery. In contrast, nanoparticles can be constructed for non-direct drug administration. Therapeutic drugs can treat sight-threatening retinal diseases at specific sites. This delivery strategy is still being investigated for efficacy and safety [26]. To combating this, Poly(lactic-co-glycolic acid)-PLGA and Polylactic acid- PLA are attractive delivery carriers because to their stability, biocompatibility, and biodegradability, according to research. To reduce dosage and frequency, PLGA polymeric nanoparticles increase drug release and reduce eye discomfort. There has been great interest in developing sustained anti-VEGF delivery systems in a bid to reduce the frequency and risks of multiple intravitreal injections. Intravitreal injection (IVT) of anti-vascular endothelial growth factors (VEGF) (such as aflibercept, ranibizumab, and bevacizumab) effectively treats neovascular AMD, but it's still invasive. Thus, biologic drug delivery methods are popular in academics and industry. Therefore, using innovative drugs delivery methods is crucial [27–40].

In light of the fact that ocular drug delivery using nanomicelles has been widely explored for various ocular indications due to the advantages like controlled drug release, effective crossing of ocular barriers and improved bioavailability with minimal ocular toxicity [41,42]. Nanomicelles, due to their unique structure, can encapsulate highly hydrophobic drugs and enhance their solubility. This can facilitate in drug penetration and effective drug delivery to the target tissue. Mixed amphiphilic nanomicelles demonstrate a stronger hydrophobic interactions and stronger hydrogen bonding with the adjacent polymers [43]. Ophthalmic drugs, such as Ranibizumab, are hydrophobic; however, the nanomicelles made with grafted co-polymer overcome this property, making them ideal for topical delivery as aqueous-based solutions. When concentration exceeds critical micelle concentration, self-assembly occurs. These features also make the technique easily adaptable to large-scale preparation, if desired. Several studies reported that copolymer based nanomicelles formulations and its action [44–47]. In this study, we have utilized a mixture of co-polymers; PLGA/PLA for the nanomicellar formulation. These polymers are classified as “Generally Regarded as Safe” (GRAS) by the US-FDA. Clear nanomicellar solutions of hydrophobic drugs can be suitable for topical administration and for intravitreal administration due to their clarity [48]. In order to increase the long-acting intraocular administration for macular degeneration, the present study sought to produce a unique fabrication of PLGA/PLA co-polymeric nanomicelles loaded ranibizumab drug to reduce inflammation and oxidative stress in retinal pigmented epithelilal cells, which is the first sign of macular degeneration. For this, we developed a nanomicellar formulation of ranibizumab (Rabz) using an optimized mixture of two polymers, PLGA/PLA which were characterize via FTIR, XRD, TEM, DLS and Zeta potential. An *in vitro* drug release study of Rabz-CP-NMs was performed. *In vitro* cell cytotoxicity, *in-vitro* cellular uptake of Rabz-CP-NMs as compared to drug (Rabz) were evaluated using various ocular cell lines. Finally, the *in vitro* bioactivity of Rabz-CP-NMs was performed using sodium iodate induced inflammation and reactive oxidative stress on retinal pigment epithelial cells.

2. Materials and methods

2.1. Chemicals

For the polymer synthesis, PLGA (MW, 12000 kDa, 50:50), PLA (Mw = 72,200 ± 15,000 Da), Tin(II) 2-octoate and $CH_3(CH_2)_{11}OH$ (1-dodecanol) were utilized. Else, N,N-dicyclohexyl carbodi-imide (DCC), N-hydroxy succinimide (NHS), Dimethyl Sulfoxide (DSS), Sodium hydroxide (NHS), Acetone, Potassium hydrogen phosphate, NaCl and $CaCl_2 \bullet 2H_2O$, NaOH, and $NaHCO_3$ all of which were bought from Sigma–Aldrich Chemicals. The AnnexinV/FITC and PI Staining, fluorescein isothiocynate (FITC), ELISA kits and dialysis membrane were procured from Thermo Fisher Scientific Inc. (USA). Unless then stated, all the chemicals were graded analytical reagents.

2.2. Fabrication of CP-NMs

The PLGA/PLA copolymers nanomicelles (CP-NMs) were fabricated by ring-opening polymerization (ROP) method described by Song et al. [49,50]. Briefly, PLA: 5.0 g and PLGA: 3.7520 g, were put into a round-bottomed flask with 0.02 % tin-octanoate catalyst (of the total dimers mass) and 0.01 % 1-dodecanol initiator. To initiate the catalyzed polycondensation reaction, the flask was placed in a preheated oil bath at 170–180 °C. Magnetic stirring was employed throughout the synthesis to provide improved homogeneity. After 2 h the products was poured into a sealed flask in a refrigerator at −20 °C.

2.3. Assessment of CMC

As a hydrophobic probe, iodine was used to estimate the CMC of the CP-NMs. A standard iodine/potassium iodide solution was prepared for the experiment by mixing 50 ml of distilled deionized water with 1:2 iodine and potassium iodide [51,52]. In dH_2O, the CP-NMs was made at dose ranging from 1 to 40 μg/ml. The diluted polymer solutions were mixed with 25 μl of I2/KI solution and incubate in the dark room temp at 24 h. It follows that the UV absorbance of different diluted concentrations was measured and recorded at 366 nm after the incubation time. A graph interpolating the absorbance against the polymer concentration (μg/ml) displayed the values. The CMC was determined by taking the interface of the points where the absorbance grew rapidly and the absorbance remained constant; a rise in iodine concentration was indicative of an increase in micelle concentration.

2.4. Preparation of ranibizumab (Rabz) loaded CP-NMs

Ranibizumab (Rabz), an anti-VEGF drugs, was loaded into CP-NMs adopting the nano-precipitation technique [53]. To prepare a homogeneous solution, 15 ml of acetone was used to dissolve 60 mg of CP-NMs and 3 mg of ranibizumab. After that, the surfactant

Pluronic F-68 (1.5%) was added to 50 ml of water using a syringe, and the combined solutions were stirred moderately. Instantaneously, Rabz-CP-NMs were synthesized. Using a Rotary Evaporator (IKATechnology, Inc., Northridge, CA), the acetone was removed from the mixture. The newly produced nanomicelles were collected by ultracentrifugation, washed three times with distilled water, and then lyophilized (Beckmann Coulter, CA).

2.5. Characterization of Rabz-CP-NMs

2.5.1. FTIR and XRD analysis

The FTIR spectra of PLGA, PLA, Rabz, CP-NMs, Rabz-CP-NMs were obtained (Bruker ALPHA II compact, Germany) at 4000 and 400 cm^{-1}. The samples were prepared by spreading on the KBr-pellet. The PXRD analysis was used to evaluate the distribution of PLGA, PLA, Rabz, CP-NMs, and Rabz-CP-NMs. The D8-Advance Bruker-AXS diffractometer was used to obtain the XRD patterns by Cu Kα irradiation. It was performed in continuous mode at a speed of 4°/min within the 2θ range of 5–40°.

2.5.2. TEM, DLS and Zeta potential analysis

Morphological studies of the Rabz-CP-NMs were examined by TEM (JEOL 1011, and Japan). The Rabz-CP-NMs were dropped onto a microscope grid coated with copper with 0.5–0.05 % w/v drug doses, respectively. The particle size of Rabz-CP-NMs (0.5 mg/ml) was used to examined by DLS at room temperature (Beckman Coulter, Inc. Delsa™). The surface charge of the Rabz-CP-NMs (0.5 mg/ml) were examined by zeta potential Zeta-sizer Nano ZS (UK) at ambient temperature.

2.6. Drug release activity

The impact of drug release were conducted to examine the release of Rabz from fabricated Rabz-CP-NMs. A solution of 5 ml of freshly prepared PBS with a pH- 7 and 0.1 mg/ml of bovine pancreatic protease (Sigma, Germany) was used to disperse the weighted nanomicelles (10 mg). Purposefully simulating the intracellular milieu, where peptide bonds are hydrolyzed by proteases [54,55]. The 22 mm × 20 mm pretreatment dialysis membrane (MWCO 3500 Da, Serva) was used to collect the solution. Placing the dialysis tubing in a beaker with 100 ml of newly made PBS at a pH-7 followed by sealing it with Teflon clips. While incubating at 37 °C, the resulting solution was continuously shaken at 90×*g* using a rotary shaker. The pattern of slow release was stable for up to 48 h. At regular intervals, a volume of one milliliter of the reaction mixture was withdrawn. The UV-Visible spectra (Perkin-Elmer) was used to estimate the Rabz emitted, with a maximum wavelength of 450 nm.

2.7. In vitro cytoviability assay

2.7.1. Cell culture

D407 and ARPE19, two types of macular pigmented epithelial cells, were obtained from the ATCC and maintained in RPMI with 10% FBS at 37 °C in a humidified atmosphere with 5% CO2. The ocular cells had been trypsinized with a PBS solution until they reached 70% confluence in their tissue culture flask.

2.7.2. MTT assay

Ocular cells D407 and ARPE19 were used to assess the cellular cytotoxicity of Rabz, CP-NMs, and Rabz-CP-NMs by MTT assay [47]. A cell density of 1×10^4 cells/well was used to seed ninety six well plates, and 200 μL of full DMEM was used to suspend the cells. Triton-X (5%: $^{(+)}$ control) and blank (SFM: $^{(-)}$ control), CP-NMs, Rabz drug alone and Rabz-CP-NMs doses of 20–100 μg/mL at 24 h. The % of viability of ocular cells were estimated = Abs of sample − Abs of $^{(+)}$ control/Abs− Abs of $^{(-)}$ control x 100. They were subsequently fixed on a microscope slide and examined for alterations in ocular cell shapes using phase contrast and fluorescence microscopy to determine their impact on mitochondrial function.

2.7.3. Cell proliferation assay

The quantity of alive cells was determined using the CCK-8-cell counting kit made by Dojindo Molecular of Japan. The D407 and ARPE19 (5000 ocular cells) were placed to each well and incubated at 37 °C with 5% CO_2, at 72 h which was then propagated into cover slips and subjected to dose of 1 mg/ml CP-NMs, Rabz drug alone, or Rabz-CP-NMs for 24 h. The results were then evaluated. In order to measure optical density (OD), a microplate reader (Spectra Max M5, USA) maintained a constant wavelength of 450 nm. Afterwards, the ocular cells were subjected to a cold PBS wash, fixed for 15 min at room temp with 4% formaldehyde and labelled with 1 mg/mL acridine orange. Fluorescence microscopy (Olympus Optical, Tokyo, Japan) at 40 × mag was used to visually examine cell proliferation after 10 min of incubation.

2.8. In vitro cell uptake studies

For the purpose of studying cellular uptake, Rabz, CP-NMs, and Rabz-CP-NMs in ARPE19 and D407 ocular cells were identified by FITC labelling as per the protocol [47]. To begin with, 5×10^4 ocular cells were propagated into a 24-well plate. Next, each well was supplemented with 20 μL of FITC-tagged Rabz, CP-NMs, and Rabz-CP-NMs with a period of 6–24 h. It was washed twice with DPBS at each time point. The cells were then spun twice for 5 min at 20,000 rpm in FACS tubes after they were obtained. Finally, DPBS was utilized as to make the sample. Using FACS at 490 nm, the untreated cells, Rabz, CP-NMs, and Rabz-CP-NMs subjected cells were compared to their mean fluorescence intensity.

The morphology of D407 and ARPE19 ocular cell uptake was also determined through fluorescence microscopy. Methods for labeling FITC to Rabz, CP-NMs, and Rabz-CP-NMs are detailed above. Following that, 10 μL of Rabz, CP-NMs, and Rabz-CP-NMs were administered to every chamber, and the therapy ended after 24 h. Before being stained with DAPI dye, the ocular cells were rinsed with PBS for thrice, fixed with cold 4% buffered paraformaldehyde. Using a coverslip, the slides were covered and sealed. Following two washes with PBS, the cells were prepared for Fluoromount mounting.

2.9. Apoptosis assay

The effect of Rabz, CP-NMs, and Rabz-CP-NMs on cell death was assessed by labeling D407 and ARPE19 ocular cells with Annexin V/FITC and propodium iodide, and then figuring out the results via flow cytometry. The ocular cells were propagated in a six-well dish at a density of 2×10^1 cells. Following a 24-h attachment, the cells were subjected to 1 mg/mL of Rabz, CP-NMs, and Rabz-CP-NMs. Following 24 h of treatment, the ocular cells were takeout by centrifugation. They were subsequently detached by adding 200 μL of trypsin, rinsed twice with cold DPBS and PBS, and finally, given a final rinse. Cells were carefully collected after the 24-h period and stained according to the specified protocol using the Annexin V-FITC Apoptosis Staining Kit (Abcam). In order to evaluate the cells using flow cytometry (Millipore Corporation in Billerica, MA, USA), 5 μL of Annexin V-FITC was added to the cell suspension. After incubating the cells for 15 min in the dark, 10 μL of PI was added.

2.10. Examination of cell migration by wound scratch assay

To examine the migratory potential of D407 and ARPE19 cells were carried out by wound scratch assay. The ocular cells (3×10^6) were seeded in 60 mm culture dishes and incubated for 24 h. A wound was made in the monolayer using a sterile pipette tip once the cells reached confluence and the cells were individually exposed to 1 mg/L of the Rabz, CP-NMs and Rabz-CP-NMs. Using fluorescence microscopy, photographs of cells invading the wound were taken at the indicated times (0–72 h).

2.11. In vitro antioxidant ability of ROS by DCFDA assay

DCFDA was used to measure ROS because it combines with reactive oxygen inside the cell to produce dichlorofluorescein (DCF), a molecule with a green fluorescent tint [56,57]. An initial DCF-DA stock solution (10 mM) was made in methanol and then diluted with growth medium to a final concentration of 100 μM. Rabz, CP-NMs, and Rabz-CP-NMs (100 μg/ml) were administered to D407 and ARPE19 ocular cells for a duration of 12 and 24 h. Along with being treated, the ocular cells were also exposed to NAC, a cellular ROS scavenger which were subsequently rinsed with cold HBSS and treated with 100 μM DCFDA at 37 °C for 30 min. Fluorescence microscopy was used to study the lysed cells, which were subjected to alkaline solutions.

2.12. Anti-VEGF/ELISA-VEGF-A inhibition

The D407 and ARPE19 ocular cells were propagated in a ninety six-plate at a rate of 1×10^4 cells. A 20 μL solution of SI, with a dose of 1 mg/mL, was added to the cells and left to sit for 24 h. Afterwards, numerous treatment groups were introduced, comprising 20 μL of Rabz-CP-NMs, CP-NMs, and Rabz medicine. At 24 h, the cells supernatant medium was analyzed for pro-inflammatory cytokines (TNFα, IL1β, IL6) and VEGF-A using sandwich ELISA (e-Biosciences, USA), in accordance to the manufacturers protocol.

2.13. Statistical analysis

All the measurements were done in triplicate, and the results were expressed as arithmetic mean ± SD. At the point, the general ANOVA F-test was broke down utilizing Tukey's test for a post hoc examination. Statistical analysis of the data was assessed by student's t-test and Graph Pad Prism®® 8.4.3 software (GraphPad Software, San Diego, CA, USA). A value of significance $p < 0.05$ was considered to be significant.

3. Results and discussion

3.1. Fabrication and characterization of Rabz-CP-NMs

Employing a nanotechnology way, CUR micelles were developed in order to enhance the drug's bioavailability, stability, and prolonged release. A possible use for nanomicelles in eye therapy is as a nano drug delivery system. Research studies have proven that nanomicelles can improve the eye drugs' solubility and permeability [48,68,69]. This study demonstrated the effective synthesis of CP-NMs using the ROP reaction as a catalyst and 1-dodecanol as an initiator (Fig. 1 shows the synthesis scheme). The prepared CP-NMs were further tested for their potential as a vehicle for drug delivery. Using the nano-precipitation technique, nanomicelles were effectively produced. To our knowledge, this is the first publication to detail a novel, simple, and cost-effective process for synthesizing Rabz-CP-NMs, which have potential future uses as a vehicle for sustained intraocular delivery. Several characterisation studies further underscored the effective synthesis of Rabz-CP-NMs.

The FTIR spectra of Anti-Vegf drug-Rabz, PLGA, PLA, CP-NMs, drug loaded CP-NMs nanomicelles (Rabz-CP-NMs) are presented in Fig. 2A. Absorption bands at 3046 cm^{-1} (=C-H bending of aromatic ring), 2990 and 2530 cm^{-1} (-CH3 stretching), 780 cm^{-1} (C-H bending of naphthyl ring), and 908 cm^{-1} (-C-H bending of pair di-substitution of aromatic ring) are identified in the FTIR spectra of PLGA. The main absorption peaks of the PLA FTIR spectrum can be seen at 1735 cm^{-1}, 2864 cm^{-1}, and 1107 cm^{-1}, respectively, and correspond to the -C-O-C bending of alicyclic ethers, alkanes, and ester groups. With a wide -O-H stretching band at 3000–3700 cm^{-1}, the physical mixture revealed spectral similarities to Rabz and CP-NMs. The characteristic absorption bands of Rabz-CP-NMs shows that N–H stretching vibrations at 3512 cm^{-1} while linkages in polymer backbone was confirmed by-NH-CO-vibration band at 1393 cm^{-1}. The obvious presence of esters in the polymer chain was verified by the vibration band at 1736 cm^{-1}. The FTIR spectra of the Rabz-loaded CP-NMs formulation showed no absorption bands of Rabz because the drug was dissolved and encapsulated in the nanomicelles [70]. This finding is in strong agreement with previous research that used a ROP method to create a triblock copolymer [PCL-PEG-PCL] [31].

The XRD as displayed in Fig. 2B, CP-NMs was similar to that PLGA and PLA, and there were no typical crystal peaks of Rabz which were observed at 5° to 60° (2θ). It can be concluded that Rabz was encapsulated in the CP-NMs in the form of an amorphous state rather than the free crystal drug. This suggests that the entrapped and conjugated drug forms are in an amorphous state because they are unable to form a crystal lattice inside the polymer. All of these signs point to the drugs being dispersed throughout the nanostructure, which is the most important thing for a good DDS [71,72].

In Figs. 3 and 4A, B the distribution of sizes of Rabz-CP-NMs was displayed. It was suggested that the surface charge of Rabz-CP-NMs was almost neutral by their zeta potential of around −0.71 mV. The average size is 26.29 nm, and the size distribution patterns are relatively narrow. The morphology of the generated nanomicelles was studied under TEM and was 10–50 nm in size, with a smooth surface and a spherical form. Micelles stand out on the TEM grid as distinct, luminescent spherical globules. There was concordance between the particle sizes seen by TEM and DLS. Despite its water-like appearance, the formulation reveals mixed nanomicelles filled with drugs. In contrast to the polymers, an assembly of HCO-40 along with OC-40 produced nanomicelles which were appropriate for ocular delivery of drugs since their size was less than 40 nm [43,73,74].

When considering the nanomicelles from a pharmacological perspective, their shape is crucial. Due to their strong propensity to entangle, particles having a cone or crystal-like shape can influence pharmacokinetic parameters and the drug release profile. Conversely, it is thought that, particularly in terms of drug distribution, particles with a spherical morphology are superior. Prior research also corroborated the generated nanomicelles spherical shape [75].

3.2. Assessment of CMC

Drug bioavailability is influenced by the critical micellar concentration (CMC), a key performance indicator of the drug delivery carrier [58]. When it comes to ophthalmic applications, a higher CMC value for a specific polymer can cause the drug to release sooner than expected. This has the potential to cause the loss of

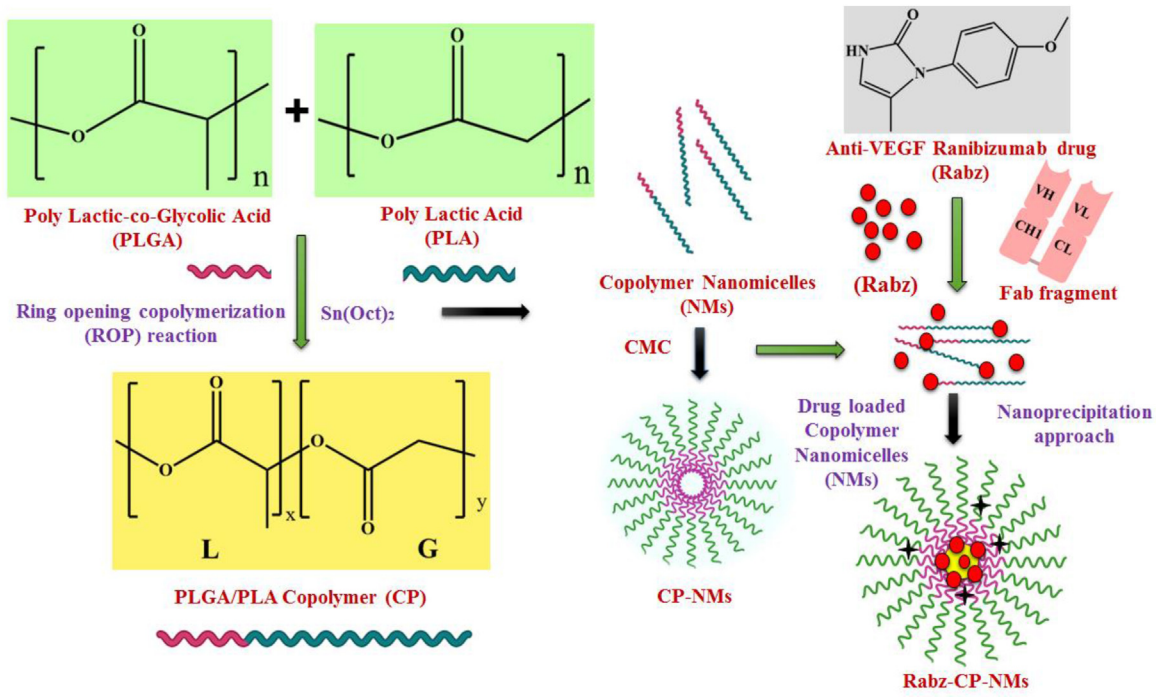

Fig. 1. Scheme representing the synthesis of Anti-VEGF drug ranibizumab loaded PLGA/PLA co-polymeric nanomicelles.

ocular formulations administered topically or intravitreally as well as the early release of the drug at a non-target location [59]. One way to reduce this loss is to encapsulate hydrophobic drugs in the basis of nanomicelles that have a reduced molecular weight [60]. To avoid tear dilution-induced nanomicellar structural rupture, a nanomicellar formulation with a lower CMC value is preferable. The current investigation determined that the CMC of CP-NMs to be 6.2 μg/ml, as illustrated in Fig. 5A, which is a graph depicting the relationship between absorbance and copolymer content. Consistent with earlier findings, the CMC values discovered were acceptable [61]. Forming thermodynamically stable NMs, the copolymer was found to have an extremely low CMC value. Ocular medication administration is made safe with copolymers because of their low CMC values, which allow micelles to be generated with minimal amounts of polymer, unlike higher CMC values that require more surfactant, which could be harmful to employ. Reportedly, the CMC and thermal stability of a polymer are both affected by the length of its hydrophilic block [62,63]. The long

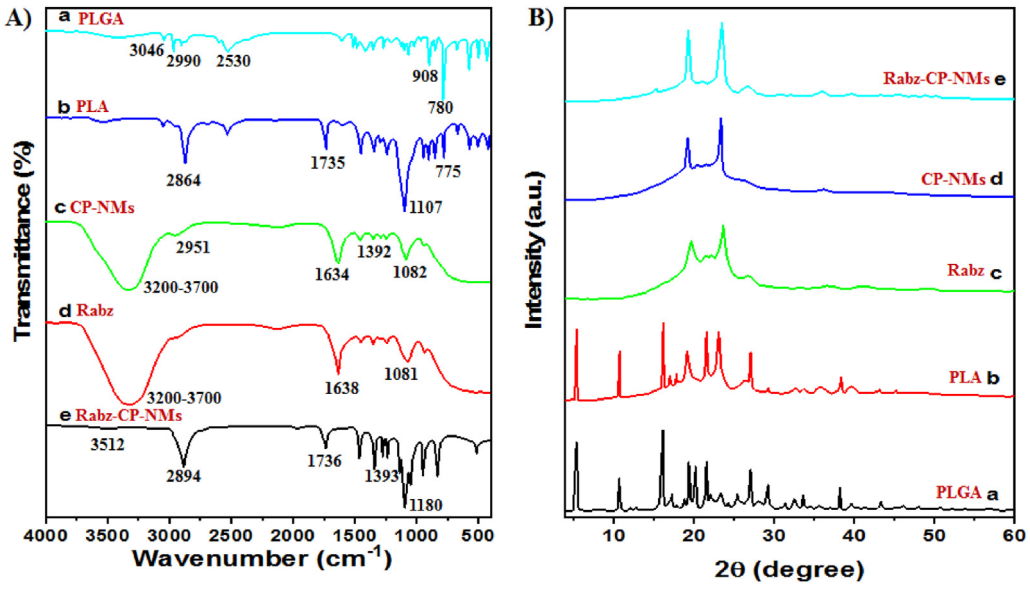

Fig. 2. A) FTIR spectra and; B) XRD patterns of a. PLGA, b. PLA, c. Copolymeric nanomicelles (CP-NMs), d. Rabz drug and e. drug loaded copolymeric nanomicelles (Rabz-CP-NMs).

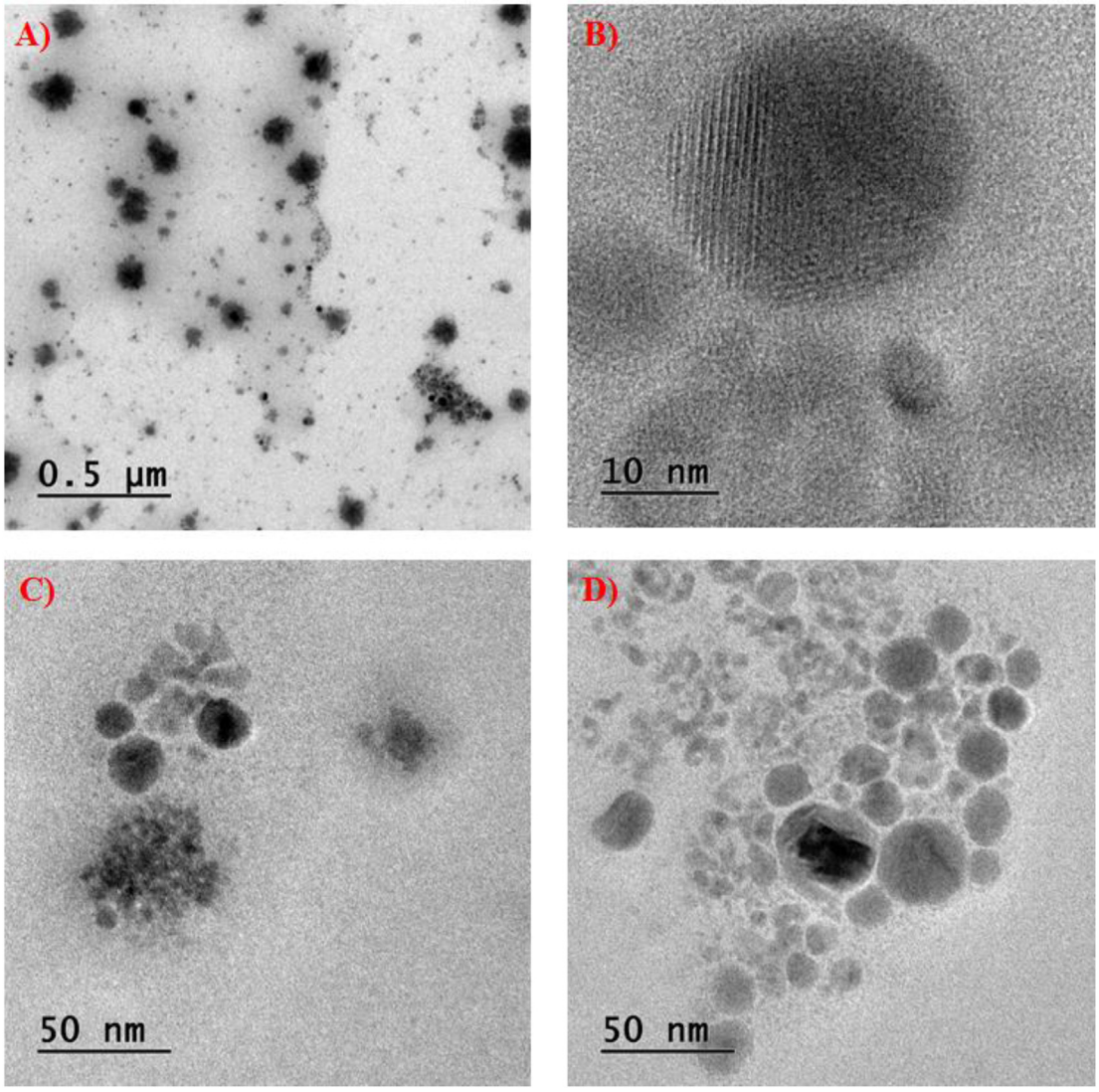

Fig. 3. The morphology of Rabz-CP-NMs: TEM images at different magnifications with spherical shape in 10–50 nm size (A,B,C,D).

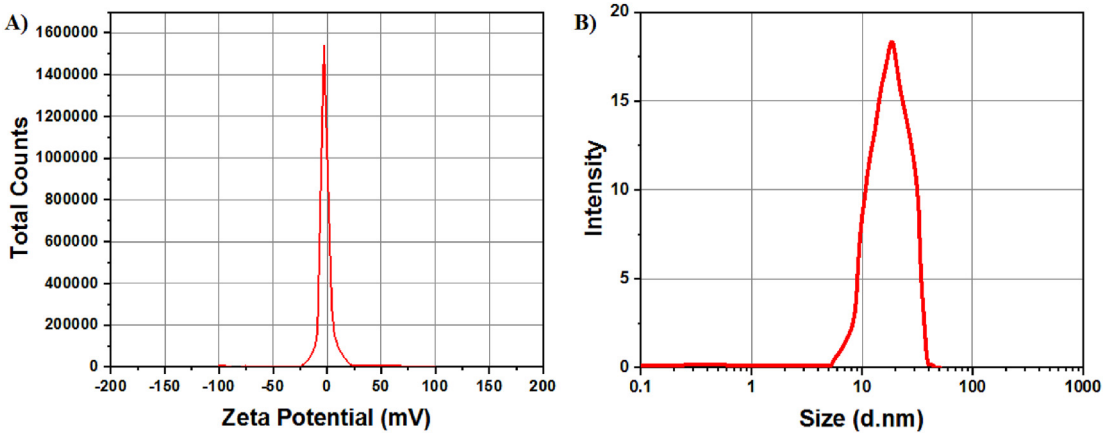

Fig. 4. The stability of Rabz-CP-NMs: A) Zeta potential analysis and; B) Size distribution of Rabz-CP-NMs by DLS.

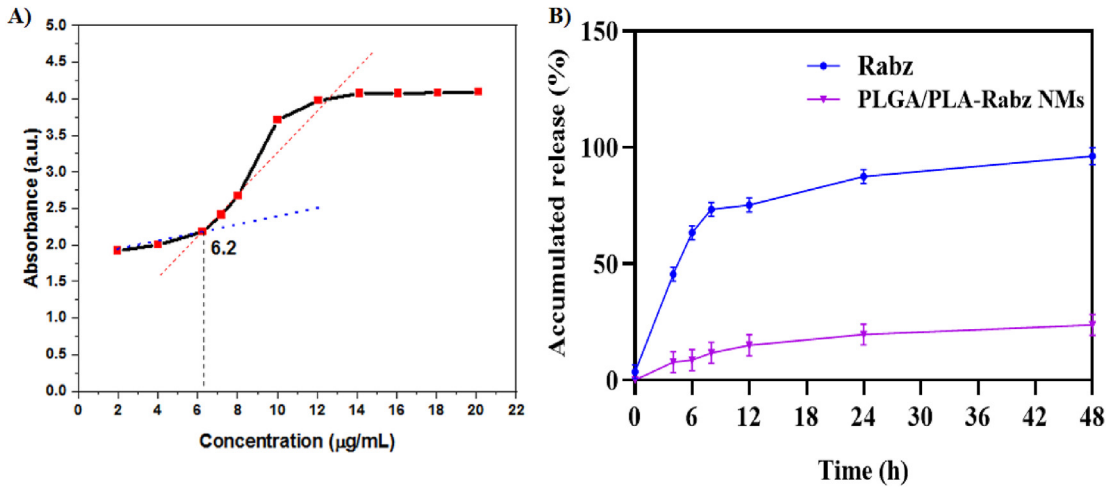

Fig. 5. A) The Critical Micelle Concentration (CMC) of copolymeric nanomicelles (CP-NMs) and; B) *In vitro* drug release of ranibizumab from Ranibizumab loaded copolymeric nanomicelles (Rabz-CP-NMs).

hydrophobic chain of the polymer is responsible for its low CMC value. Some have postulated that the stability of the produced nanomicelles is inversely related to CMC. As the CMC value decreases, the produced nanomicelles become more stable and resistant to breakage caused by fast dilution. Hence, on the basis of lower CMC, it is proposed that the prepared CP-NMs is very suitable for the efficient drug loading and drug delivery to the systemic circulation [64–67].

3.3. Drug release activity

The study of *in vitro* release supported the controlled release of Rabz from the physiological pH 7.4 of Rabz-CP-NMs, as shown in Fig. 5B. In comparison, the drug release of Rabz from Rabz-CP-NMs reaches at 23.7 % at 48 h but in the case of Rabz, it reaches 96.2 %. It indicating that the use of CP-NMs in drug delivery causes a slow and long-term release of the drug. This indicated that Rabz-CP-NMs

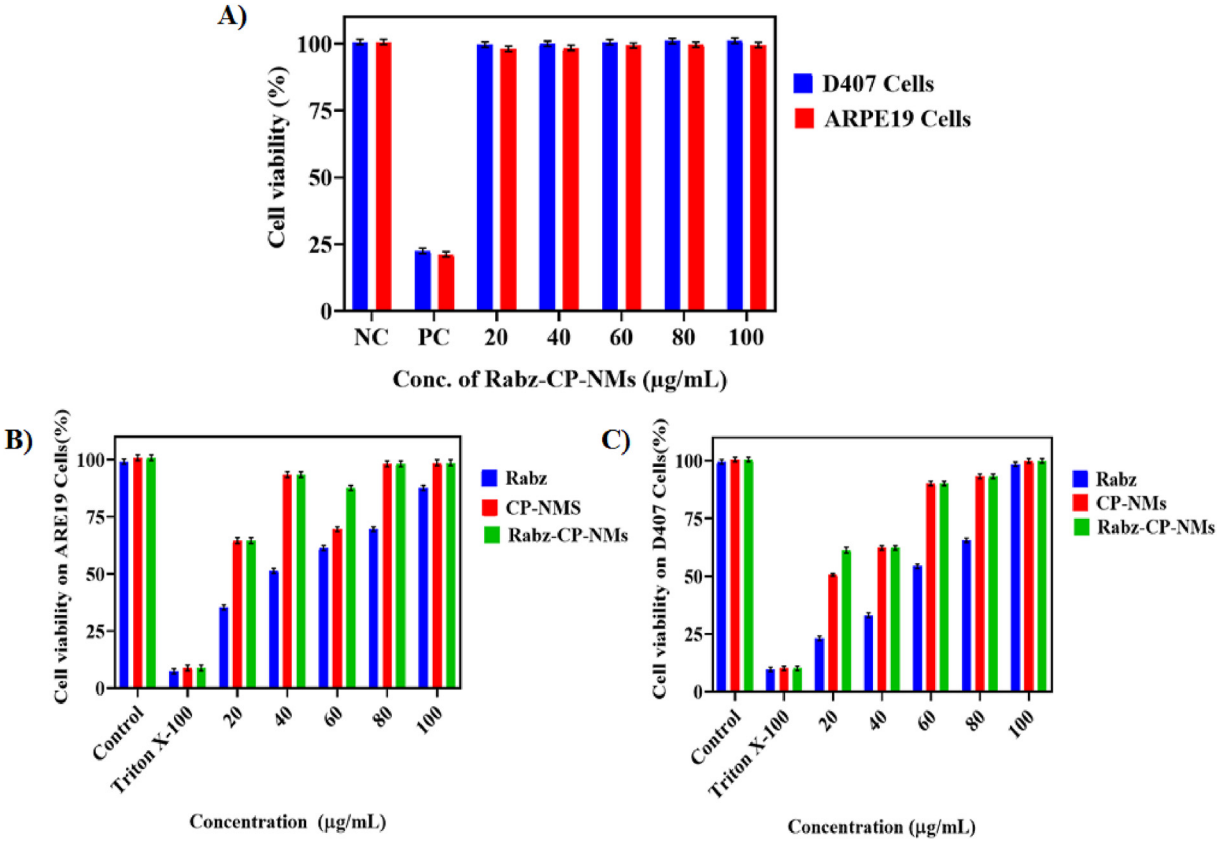

Fig. 6. *In vitro* cell viability assessment by MTT assay: A) Cell viability (%) of D407 and ARPE19 cells after treatment with Rabz, CP-NMs (20–100 μg/ml) at 24 h; Comparison of B) Cell viability (%) of D407 ocular cells after treatment with Rabz, CP-NMs and Rabz-CP-NMs at 24 h; C) Cell viability (%) of ARPE19 ocular cells after treatment with Rabz, CP-NMs and Rabz-CP-NMs at 24 h. Data are presented as mean ± standard deviation (SD). $*p \leq 0.05$ in comparison to the respective control.

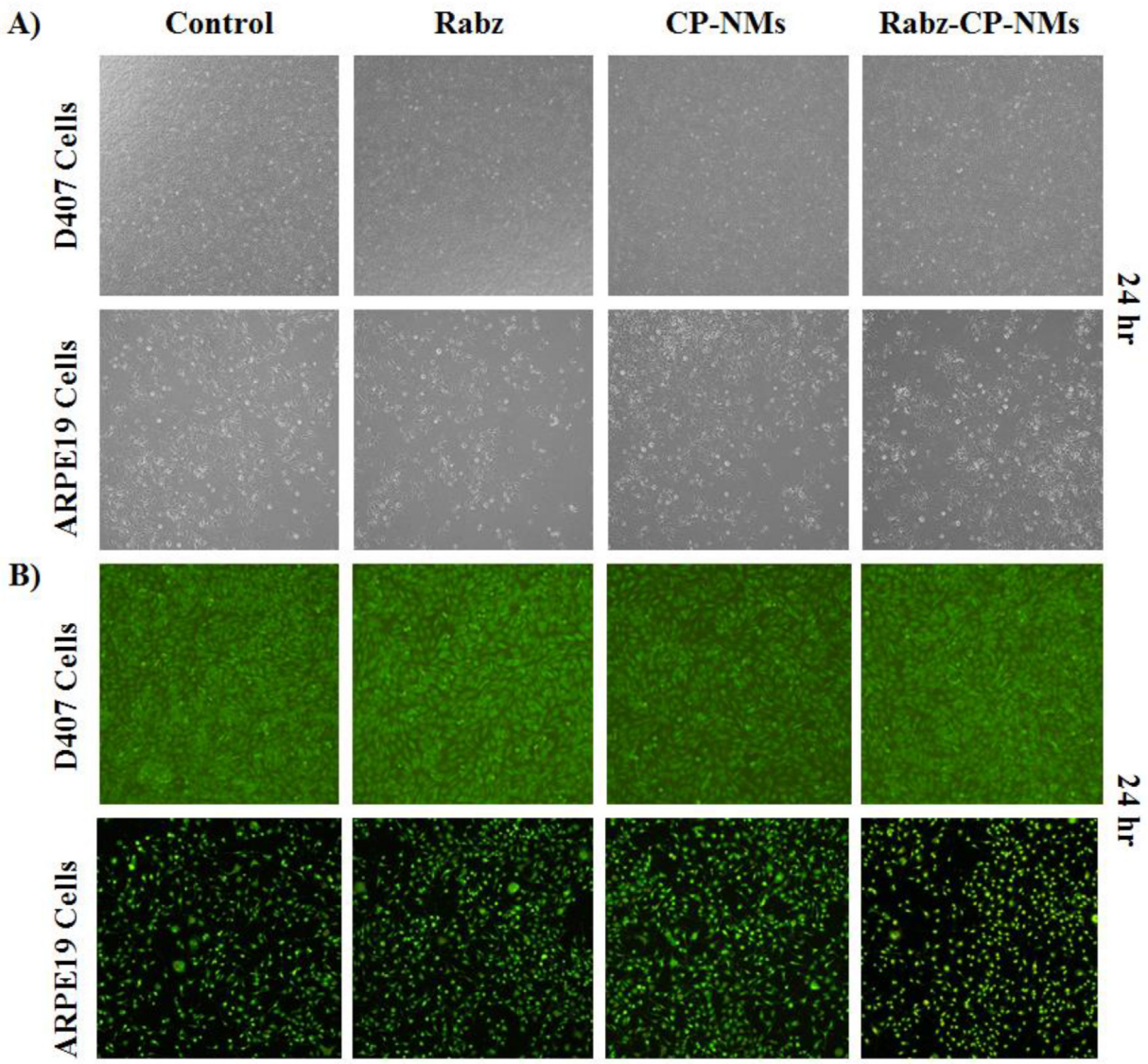

Fig. 7. Morphological examinations of cell viability: A) Phase contrast microscopic images and: B) Fluorescence microscopic images on D407 and ARPE19 ocular cells after treatment with Rabz, CP-NMs and Rabz-CP-NMs at 100 μg/ml for 24 h.

had a better controlled-release characteristic in their *in vitro* distribution profile. Increased drug acceptability, decreased drug side effects, and increased drug frequency are all possible outcomes. Likewise with the findings of Ashwinikumar et al. [76], which documented the drug delivery pattern of nanomicelles loaded with 5-FU and MTX, these results show that 75% of the controlled release PBP copolymer is present at 900 min. Also, according to Peppas's concept of drug release, the release pattern was present in all of the combinations tested [77].

3.4. *In vitro cytoviability*

Rabz, CP-NMs, and Rabz-CP-NMs were tested for *in vitro* cytotoxicity on ARPE and D407 ocular cells. The purpose of this research was to determine whether Rabz-CP-NMs and its constituents were safe for use with ocular cells. Molecular biology techniques such as the MTT cell proliferation assay, cellular uptake assay, apoptotic flow cytometry assay, and antioxidant ability of ROS by DCFDA assay were used to examine cell viability after treatment with the cells. Additionally, the inhibition of VEGF-A by anti-VEGF/ELISA was evaluated.

3.4.1. *MTT assay*

In this assay, viability of cells was assessed with Rabz, CP-NMs and Rabz-CP-NMs on D407 and ARPE19 ocular cells for 24 h. In Fig. 6A illustrates that 90 % cell viability and nontoxic effect of the Rabz-CP-NMs on D407 and ARPE19 cells at 100 μg/ml when compare to the control. The % of cell viability was found to increase in dose dependent and time dependent manner as seen from Fig. 6B and C on both ocular cells. At 100 μg/ml of Rabz-CP-NMs was found to be 99.9 % on D407 cells whereas as 98.6% on ARPE19 cells which calculated from the dose response curve. In Fig. 7A and B displayed the morphology of D407 and ARPE19 ocular cells when exposed to

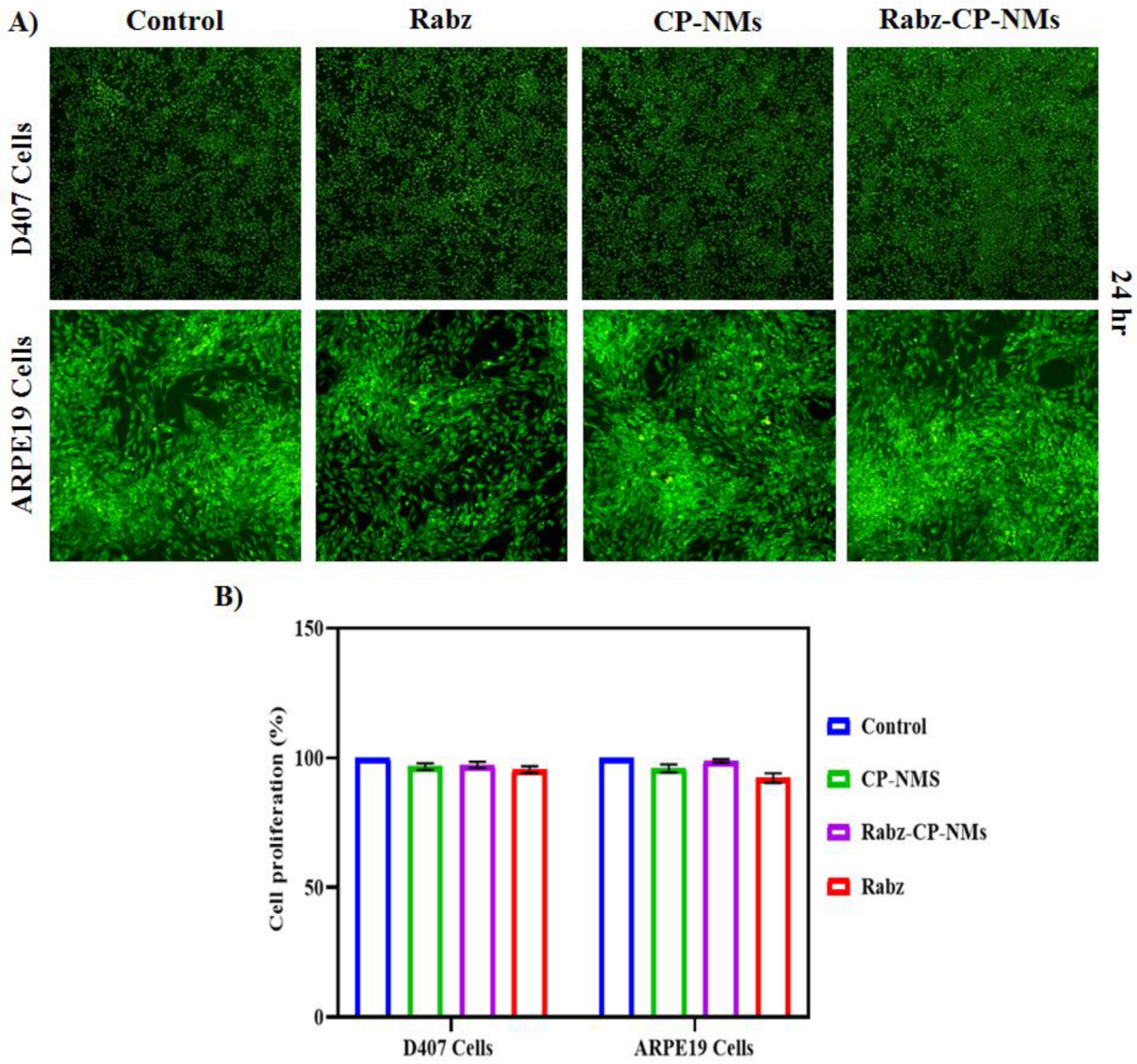

Fig. 8. Cell proliferation determination by CCK-8-cell counting kit: A) Acridine orange stained fluorescence images and; B) Percentage of proliferated D407 and ARPE19 ocular cells after treatment with Rabz, CP-NMs and Rabz-CP-NMs at 1 mg/ml for 24 h.

Rabz,CP-NMs and Rabz-CP-NMs at 24 h. It shows no alteration in cell structure and influence the cell viability at 100 μg/ml.

3.4.2. Cell proliferation

With the intent of assessing cell proliferation, to anticipate the no. of cells after 24 h subjected to the dose of 1 mg/ml of Rabz, CP-NMs, and Rabz-CP-NMs which were imagined under fluorescence microscopy (Fig. 8A). As it can be observed, Rabz, CP-NMs, and Rabz-CP-NMs influence the cell proliferation as compared to control cells. Also, as seen in Fig. 8B, cells that were exposed to Rabz-CP-NMs proliferated more rapidly than cells that were untreated at 24 h.

3.4.3. In vitro cell uptake studies

The cellular uptake of Rabz, CP-NMs and Rabz-CP-NMs were determined on D407 and ARPE19 cells to figure out the distribution of the NMs underneath the ocular cells (Fig. 9A). This investigation additionally served to compare the drug intake in Rabz alone from Rabz-CP-NMs. As seen in Fig. 9B and C, the mean fluorescence intensity of FITC-labelled Rabz-CP-NMs was statistically higher than the corresponding control and FITC-labelled Rabz treatment groups in both ocular cells at 24 h. The internalization of Rabz-CP-NMs in these cells increased with time and similar results were obtained in both the cell lines. Conversely, a weaker fluorescence for FITC-labelled Rabz was seen in the entire cell lines at all the time points as compared to the FITC-labelled Rabz-CP-NMs group. This indicates that the Rabz-CP-NMs is more rapidly absorbed by the ocular cells compared to the equivalent drugs. This is because the amphiphilic polymers bind to the cell lipid bilayer more strongly. The results of the FACS study can be matched to the results of the CLSM analysis of Rabz-CP-NMs compared to Rabz. The outcomes corroborated those of a prior publication [43] that addressed the cellular uptake of cidofovir pro-drug nanomicelles in cornel and retinal cells. Furthermore, there was an uptake rate that varies with time, as were seen with TAC and TAC-NMF [47].

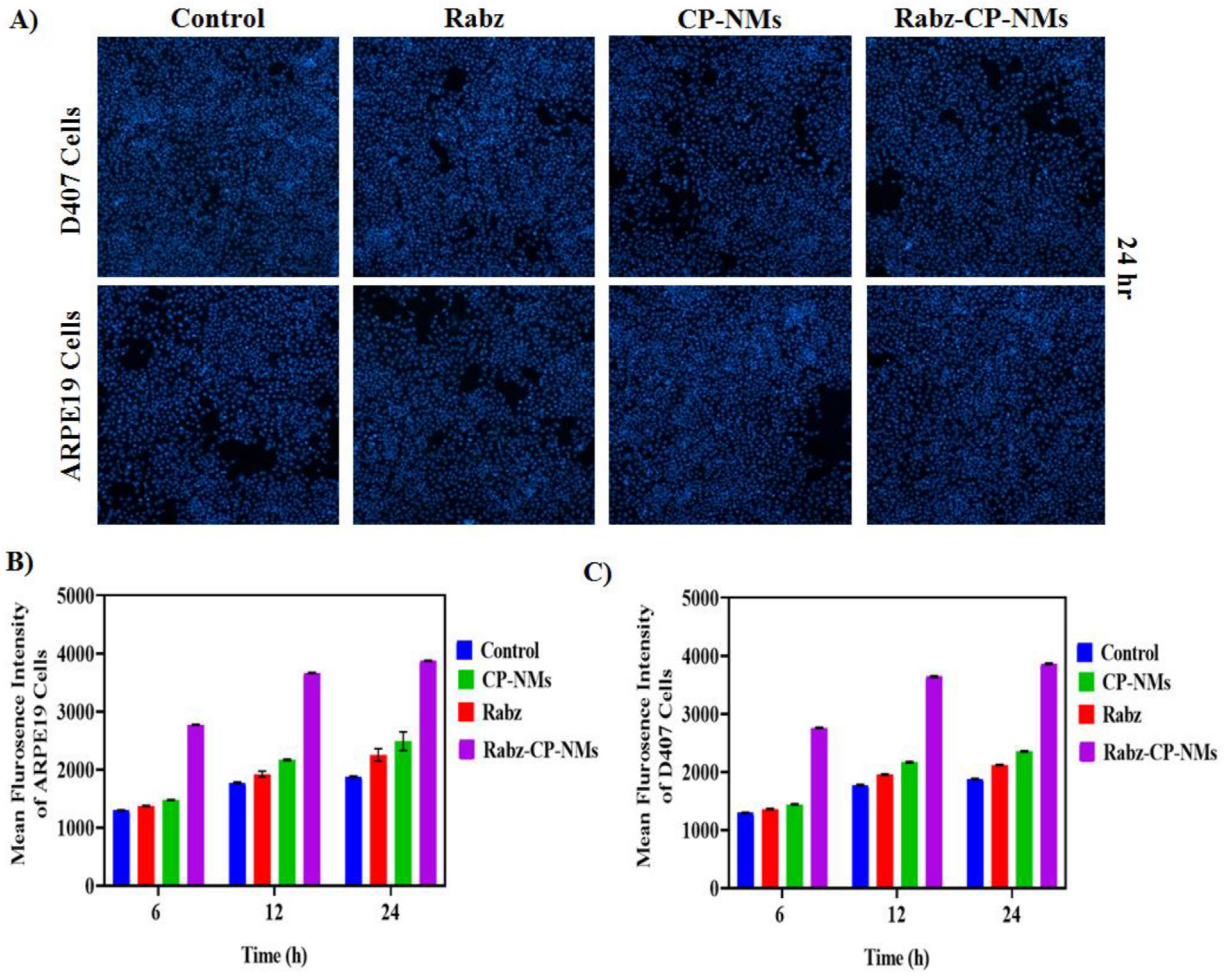

Fig. 9. Time dependent cellular uptake of FITC-labelled Rabz, CP-NMs and Rabz-CP-NMs: A) DAPI stained fluorescence images of D407 and ARPE19 ocular cells after treatment at 24 h; B) Mean fluorescence intensity of ARPE19 ocular cells and; C) Mean fluorescence intensity of D407 ocular cells. Data are presented as mean ± standard deviation (SD). $*p \leq 0.05$ in comparison to the respective control.

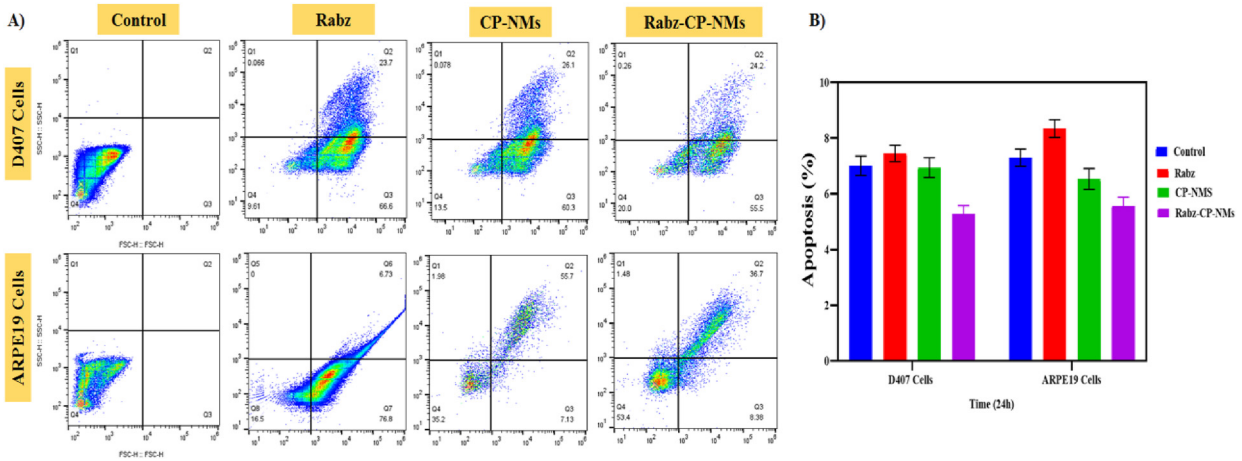

Fig. 10. Determination of apoptosis in D407 and ARPE19 ocular cells after subjected to Rabz, CP-NMs and Rabz-CP-NMs: A) Flow cytometry images by Annexin V/FITC and PI-Staining and; B) Percentage of cell apoptosis (%) at 24 h determined by FACS. Results are expressed as a mean ± standard deviation (SD). $*p \leq 0.05$ in comparison to the respective control.

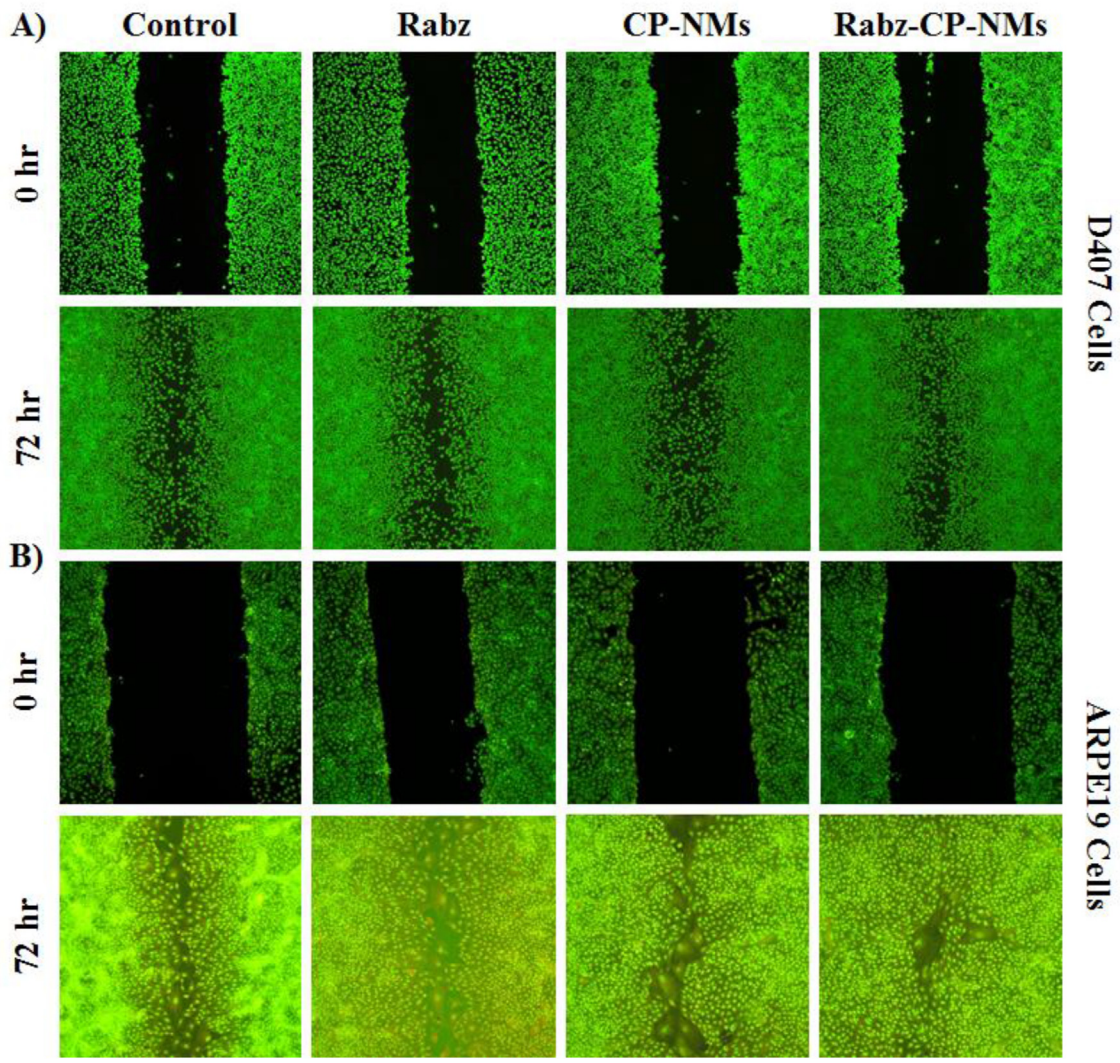

Fig. 11. Fluorescence images for determination of cell migration by wound scratch assay: A) D407 cells and; B) ARPE19 cells at 0–72 h subjected to Rabz, CP-NMs and Rabz-CP-NMs.

3.4.4. Apoptosis assay

The apoptotic effects of Rabz, CP-NMs, and Rabz-CP-NMs on D407 and ARPE19 ocular cells were tested using a flow cytometric assay at 24 h. The percentage of cells that have undergone apoptosis following treatment with Rabz, CP-NMs, and Rabz-CP-NMs in D407 and ARPE19 RF/6A ocular cells is shown in Fig. 10A. Labelling with Annexin V/FITC and PI allows for the detection of cells that have entered the late stage of cell death. Both the control and treatment groups exhibit very similar percentages of apoptotic cells. Inferring from this, it appears that the tested samples do not significantly induce cell death when exposed. Treatment with increasing concentrations of Rabz-CP-NMs resulted in a reduced percentage of cells undergoing apoptosis in both cell lines compared to the control group, as shown in Fig. 10B. Curiously, this percentage is reduced across the board in the cell lines treated with CP-NMs. An indication that the regulated release of the drug may be responsible for making Rabz drugs less harmful to the ocular cells is the statistically reduced % of apoptotic ocular cells in the CP-NMs group.

3.5. Examination of cell migration by wound scratch assay

The ocular (D407 and ARPE19) cell migration were examined via the wound scratch assay. Through this experiment, we were able to found whether cells could migrate and heal the wound when Rabz, CP-NMs, and Rabz-CP-NMs were present. Wound repairing was visually inspected by fluorescence microscopy at 0–72 h after exposure. As in the previous experiments, we observed that cells subjected to Rabz, CP-NMs, and Rabz-CP-NMs presented a comparable migratory behavior as control cells. Fig. 11 shows that Rabz-CP-NMs migrated rapidly than the control group, which was able to mend the wound and show a significant increase in comparable to cell number in the proliferation assay.

3.6. In vitro antioxidant ability of ROS by DCFDA assay

A specific probe, DCF-DA, was used in fluorescence microscopy methods to evaluate reactive oxygen species (ROS). To

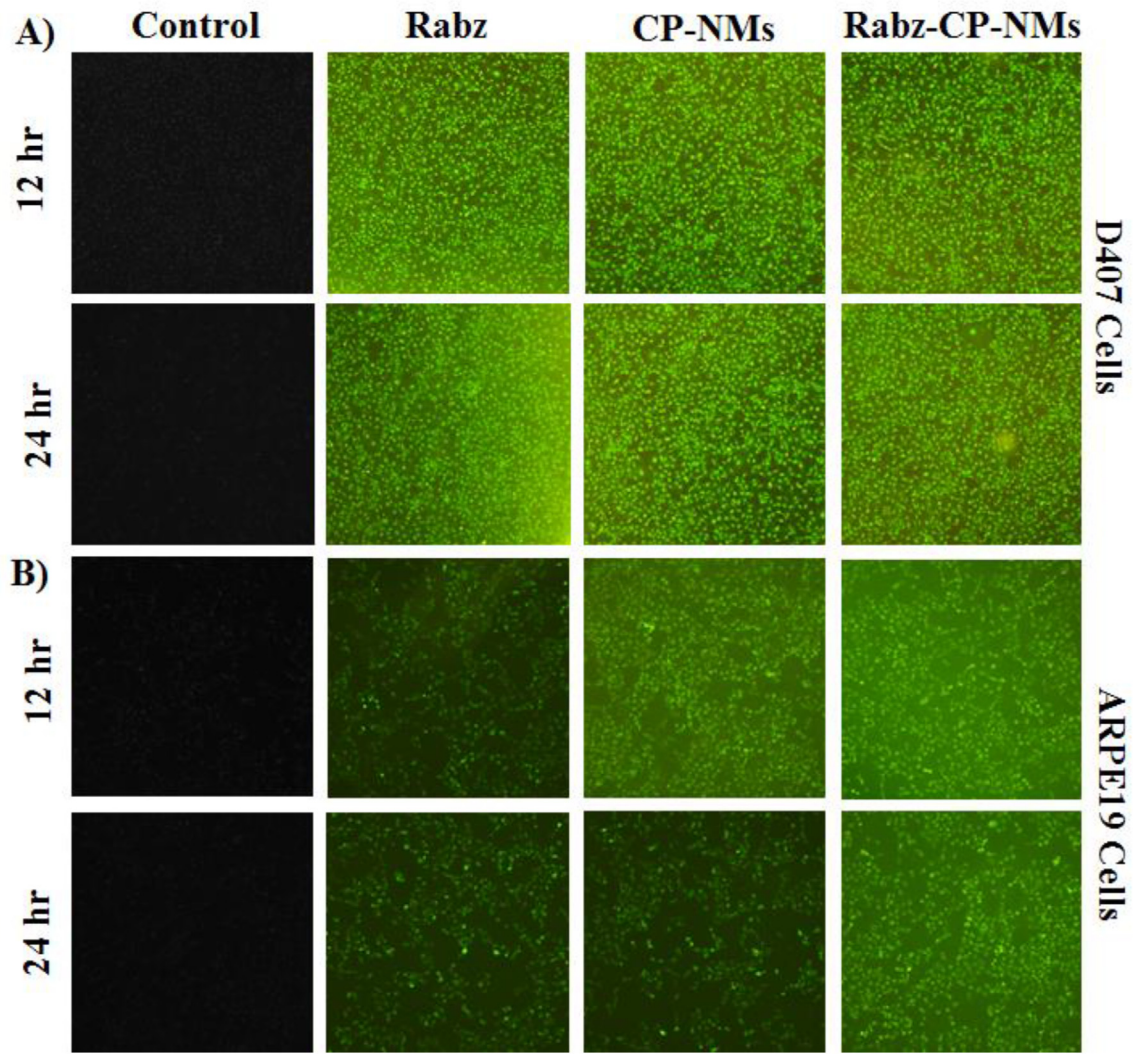

Fig. 12. Fluorescence images displays the cellular ROS by DCFDA assay: A) D407 cells and; B) ARPE19 cells at 12 and 24 h subjected to Rabz, CP-NMs and Rabz-CP-NMs.

measure ROS generation, ocular cells D407 and ARPE19 were utilized. Rabz, CP-NMs, and Rabz-CP-NMs were administered to the cells for 12 and 24 h at the appropriate doses. Results showing the average fluorescence intensity of Rabz, CP-NMs, and Rabz-CP-NMs treated ARPE19 and D407 cells for 24 h are shown in Fig. 12. Compared to control cells, ARPE19 and D407 cells subjected to Rabz-CP-NMs displayed an increase in the intensity of the green fluorescent color. The levels of ROS intensity in cells treated with Rabz-CP-NMs are considerably reversed by pre-treatment with N-acetyl cysteine (NAC), a cellular ROS scavenger. It is clear that treated cells can drastically decrease ROS production at increasing dose 100 μg/ml of Rabz and Rabz-CP-NMs at 12 and 24 h. Rabz and Rabz-CP-NMs may be able to lower ROS levels in both types of retinal pigment epithelium cells.

3.7. Anti-VEGF/ELISA-VEGF-A inhibition

The bioactivity of Rabz, CP-NMs and Rabz-CP-NMs was evaluated on D407 and ARPE19 ocular cells treated with $NaIO_3$ (SI). The oxidative stress (OS) that $NaIO_3$ causes in the RPE cells induces the demise of photoreceptors and early-stage AMD [78,79]. The first phase of AMD is considered a surge in both inflammation and OS in the retinal cells [80]. Specifically, ARPE19 and D407 cells were cultured in well plates, subjected to SI for 24 h, and then treated for further 24 h with Rabz, CP-NMs, or Rabz-CP-NMs. Using sandwich ELISA, the inflammatory cytokines found in the residual substrate, comprising TNFα, IL6, IL1β, and VEGF-A, were tested. The levels of TNFα, IL6, IL1β, and VEFG-A were decreased in the cells treated with SI compared to the control, as shown in Fig. 13A–D. This may be useful in confirming that the model is appropriate for OS induction and the subsequent release of cytokines and VEFG-A. Furthermore, across all five graphs, the SI-treated group generated somewhat greater inflammatory cytokines and VEFG-A than the Rabz-CP-NMs group. There was a concentration (20 μl) based reduction in the amounts of inflammatory cytokines and VEFG-A released by Rabz-CP-NMs and Rabz compared to the groups treated with SI and those with Rabz free CP-NMs. This indicates that the levels of TNFα, IL6, IL1β, and VEGF-A in D407 and ARPE19 cells decrease as a function of concentration following 24 h of treatment with Rabz-CP-NMs and Rabz.

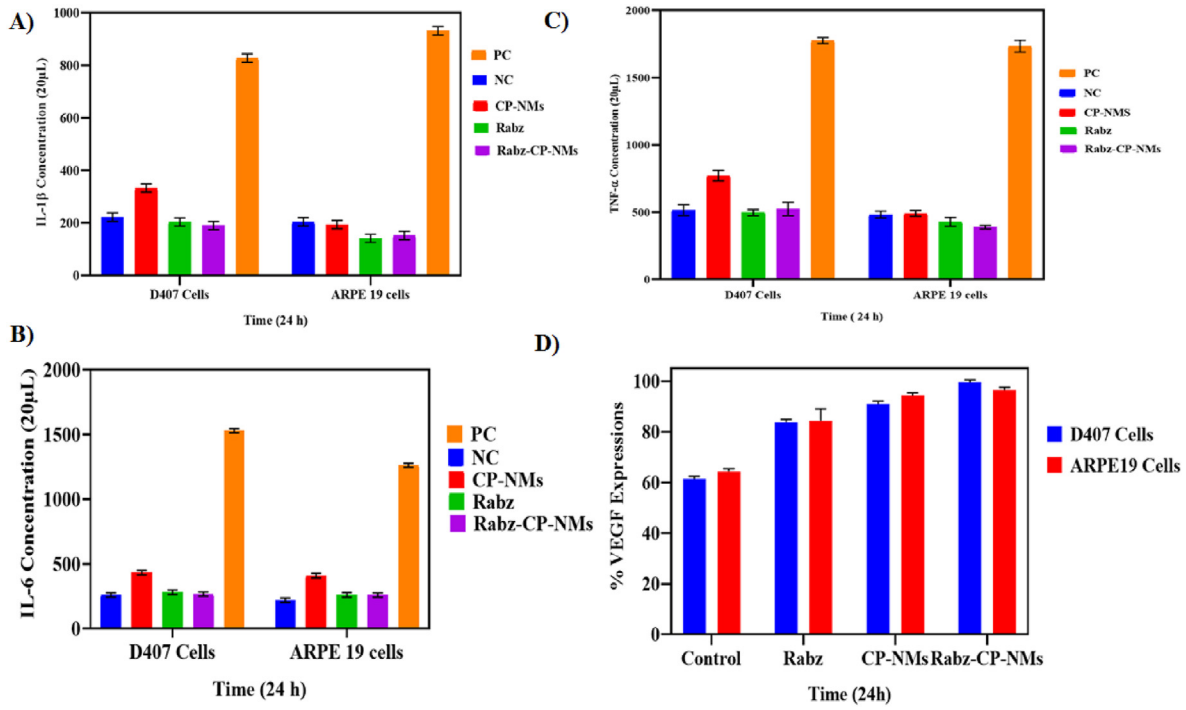

Fig. 13. *In vitro* release of: A) IL-1β; B) TNFα; C) IL-6 and; D) VEGF-A from D407 and ARPE19 ocular cells subjected with SI for 24 h exposure of Rabz, CP-NMs and Rabz-CP-NMs using ELISA. Results are expressed as a mean ± standard deviation (SD). *$p \leq 0.05$ in comparison to the respective control.

4. Conclusion

In the current investigation, fabricated the novel Rabz-CP-NMs solution which could potential to be used as an intraocular drug delivery for AMD. With a neutral charge and NMs sizes with 10–50 nm, the improved formulation maximized uptake in ocular cell lines. Both *in-vitro* dual ocular cell D407 and ARPE19 showed remarkable trans-well permeability and higher % of cell viability. It also showed the decrease levels of ROS and inflammatory cytokine which suggesting that high biocompatibility of Rabz-CP-NMs. Henceforth, the Rabz-CP-NMs showed no toxic and safe for ocular use which can could be a good candidate for improving intraocular delivery of AMD treatments.

Ethical approval

Not applicable.

Funding

Not applicable.

Author contributions

Jin-feng Xu: Materials preparation, analysis and data interpretation.

Yan-ping Wang: Data curation, Formal analysis, and Validation.

Xiao-hua Liu: Manuscript draft, Reviewing and supervision. All authors read and approved the final version of manuscript.

Data availability statement

Data will be made available on request. All the data generated or analysed during the study are included in this published article.

Consent to participate

All of the authors agree to work on this project.

Consent to publish

The approval of each author to publish the manuscript has been obtained. The manuscript is not currently under review by any other journal and has not been published before.

Declaration of competing interest

The authors declare that they have no known competing financial interests or personal relationships that could have appeared to influence the work reported in this paper.

Acknowledgments

Not applicable.

Appendix A. Supplementary data

Supplementary data to this article can be found online at https://doi.org/10.1016/j.reth.2024.06.019.

References

[1] Fine SL, Berger JW, Maguire MG, Ho AC. Age-related macular degeneration. N Engl J Med 2000;342(7):483–92. https://doi.org/10.1056/NEJM200002173420707.

[2] Dedania VS, Bakri SJ. Current perspectives on ranibizumab. Clin Ophthalmol 2015;9:533–5429. https://doi.org/10.2147/OPTH.S80049.

[3] Ba J, Peng RS, Xu D, Li YH, Shi H, Wang Q, et al. Intravitreal anti-VEGF injections for treating wet age-related macular degeneration: a systematic review and meta-analysis, Drug Design. Drug Des Dev Ther 2015;9:5397–405. https://doi.org/10.2147/DDDT.S86269.

[4] Campbell M, Doyle SL. Current perspectives on established and novel therapies for pathological neovascularization in retinal disease. Biochem Pharmacol 2019;164:321–5. https://doi.org/10.1016/j.bcp.2019.04.029.
[5] Jiang G, Han X, Qiao K, Liu S. Therapeutic effect of intravitreal anti-VEGF drugs on retinal neovascularization in diabetic retinopathy. Minerva Med 2022: 7943–5. https://doi.org/10.23736/s0026-4806.22.07943-5.
[6] Arrigo A, Aragona E, Bandello F. VEGF-targeting drugs for the treatment of retinal neovascularization in diabetic retinopathy. Ann Med 2022;54(1): 1089–111. https://doi.org/10.1080/07853890.2022.2064541.
[7] Tomita Y, Lee D, Tsubota K, Negishi K, Kurihara T, et al. Updates on the current treatments for diabetic retinopathy and possibility of future oral therapy. J Clin Med 2021;10(20):4666. https://doi.org/10.3390/jcm10204666.
[8] Lashay A, Riazi-Esfahani H, Mirghorbani M, Yaseri M. Intravitreal medications for retinal vein occlusion: systematic review and meta-analysis. J Ophthalmic Vis Res 2019;14(3):336–66. https://doi.org/10.18502/jovr.v14i3.4791.
[9] Maxwell JD, Greig WR, Boyle JA, Pasieczny T, Schofield CB. Reiter's syndrome and psoriasis. Scot Med J 1966;11(1):14–8. https://doi.org/10.1177/003693306601100103.
[10] Hitschke K, Bühler R, Apell HJ, Stark G. Inactivation of the Na, k-ATPase by radiation-induced free radicals Evidence for a radical-chain mechanism. FEBS Lett 1994;353(3):297–300. https://doi.org/10.1016/0014-5793(94)01067-6.
[11] Domańska-Janik K. Experimental hypoxia and some problems of oxygenic glucose metabolism in the central nervous system. Neuropatol Pol 1972;10(1):17–43.
[12] Brinkmann A, Winkelmann K, Käckenmeister T, Roider J, Klettner A. Effect of long-term anti-VEGF treatment on viability and function of rpe cells. Curr Eye Res 2022;47(1):127–34. https://doi.org/10.1080/02713683.2021.1931344.
[13] Zhao HY, Wu J, Zhu JJ, Xiao Z, He C, Shi H. Research advances in tissue engineering materials for sustained release of growth factors. BioMed Res Int 2015;2015:808202. https://doi.org/10.1155/2015/808202.
[14] Hayreh SS. Photocoagulation for retinal vein occlusion. Prog Retin Eye Res 2021;85:100964. https://doi.org/10.1016/j.preteyeres.2021.100964.
[15] Rosenfeld PJ, Brown DM, Heier JS, Boyer DS, Kaiser PK, Chung CY, et al., MARINA Study Group. Ranibizumab for neovascular age-related macular degeneration. N Engl J Med 2006;355:1419–31. https://doi.org/10.1056/NEJMoa054481.
[16] Brown DM, Kaiser PK, Michels M, Soubrane G, Heier JS, Kim RY, et al., ANCHOR Study Group. Ranibizumab versus verteporfin for neovascular age-related macular degeneration. N Engl J Med 2006;355:1432–44. https://doi.org/10.1056/NEJMoa062655.
[17] Brown DM, Michels M, Kaiser PK, Heier JS, Sy JP, Ianchulev T, ANCHOR Study Group. Ranibizumab versus verteporfin photodynamic therapy for neovascular age-related macular degeneration: two-year results of the ANCHOR study. Ophthalmology 2009;116:57–65.e5. https://doi.org/10.1016/j.ophtha.2008.10.018.
[18] Regillo CD, Brown DM, Abraham P, Yue H, Ianchulev T, Schneider S, et al. Randomized, double-masked, sham-controlled trial of ranibizumab for neovascular age-related macular degeneration: PIER Study year 1. Am J Ophthalmol 2008;145:239–248.e5. https://doi.org/10.1016/j.ajo.2007.10.004.
[19] Abraham P, Yue H, Wilson L. Randomized, double-masked, shamcontrolled trial of ranibizumab for neovascular age-related macular degeneration: PIER study year 2. Am J Ophthalmol 2010;150:315–324. e1. https://doi.org/10.1016/j.ajo.2010.04.011.
[20] Campochiaro PA, Heier JS, Feiner L, Gray S, Saroj N, Rundle AC, et al. Ranibizumab for macular edema following branch retinal vein occlusion: six-month primary end point results of a phase III study. Ophthalmology 2010;117: 1102–1112.e1. https://doi.org/10.1016/j.ophtha.2010.02.021.
[21] Brown DM, Campochiaro PA, Singh RP, Li Z, Gray S, Saroj N, et al. CRUISE Investigators. Ranibizumab for macular edema following central retinal vein occlusion: six-month primary end point results of a phase III study. Ophthalmology 2010;117:1124–1133.e1. https://doi.org/10.1016/j.ophtha.2010.02.022.
[22] Nguyen QD, Brown DM, Marcus DM, Boyer DS, Patel S, Feiner L, et al., RISE and RIDE Research Group. Ranibizumab for diabetic macular edema: results from 2 phase III randomized trials: RISE and RIDE. Ophthalmology 2012;119: 789–801. https://doi.org/10.1016/j.ophtha.2011.12.039.
[23] Kim TW, Lindsey JD, Aihara M, Anthony TL, Weinreb RN. Intraocular distribution of 70-kDa dextran after subconjunctival injection in mice. Invest Ophthalmol Vis Sci 2002;43:1809–16.
[24] Sakurai E, Ozeki H, Kunou N, Ogura Y. Effect of particle size of polymeric nanospheres on intravitreal kinetics. Ophthalmic Res 2001;33:31–6.
[25] Koo H, Moon H, Han H, Na JH, Huh MS, Park JH, et al. The movement of self-assembled amphiphilic polymeric nanoparticles in the vitreous and retina after intravitreal injection. Biomaterials 2012;33:3485–93.
[26] Kumari A, Yadav SK, Yadav SC. Biodegradable polymeric nanoparticles based drug delivery systems. Colloids Surf B Biointerfaces 2010;75:1–18.
[27] Bolla PK, Gote V, Singh M, Patel M, Clark BA, Renukuntla J. Lutein-loaded, biotin-decorated polymeric nanoparticles enhance lutein uptake in retinal cells. Pharmaceutics 2020;12:798. https://doi.org/10.3390/pharmaceutics12090798.
[28] Narvekar P, Bhatt P, Fnu G, Sutariya V. Axitinib-loaded poly(lactic-Co-glycolic acid) nanoparticles for age-related macular degeneration: formulation development and *in vitro* characterization. Assay Drug Dev Technol 2019;17: 167–77. https://doi.org/10.1089/adt.2019.920.
[29] Liu JX, Zhang XY, Li G, Xu F, Li S, Teng LS, et al. Anti-angiogenic activity of bevacizumab-bearing dexamethasone-loaded PLGA nanoparticles for potential intravitreal applications. Int J Nanomed 2019;14:8819–34. https://doi.org/10.2147/IJN.S217038.
[30] Li F, Hurley B, Liu Y, Leonard B, Griffith M. Controlled release of bevacizumab through nanospheres for extended treatment of age-related macular degeneration. Open Ophthalmol J 2012;6:54–8. https://doi.org/10.2174/1874364101206010054.
[31] Zhang LL, Si T, Fischer AJ, Letson A, Yuan S, Roberts CJ, et al. Coaxial electrospray of ranibizumab-loaded microparticles for sustained release of anti-VEGF therapies. PLoS One 2015;10:e0135608. https://doi.org/10.1371/journal.pone.0135608.
[32] Sousa F, Cruz A, Fonte P, Pinto IM, Neves-Petersen MT, Sarmento B. A new paradigm for antiangiogenic therapy through controlled release of bevacizumab from PLGA nanoparticles. Sci Rep 2017;7:3736. https://doi.org/10.1038/s41598-017-03959-4.
[33] Varshochian R, Riazi-Esfahani M, Jeddi-Tehrani M, Mahmoudi AR, Aghazadeh S, Mahbod M, et al. Albuminated PLGA nanoparticles containing bevacizumab intended for ocular neovascularization treatment. J Biomed Mater Res, Part A 2015;103:3148–56. https://doi.org/10.1002/jbm.a.35446.
[34] Hoshikawa A, Tagami T, Morimura C, Fukushige K, Ozeki T. Ranibizumab biosimilar/polyethyleneglycol-conjugated gold nanoparticles as a novel drug delivery platform for age-related macular degeneration. J Drug Deliv Sci Technol 2017;38:45–50. https://doi.org/10.1016/j.jddst.2017.01.004.
[35] Yan J, Peng XF, Cai YL, Cong WD. Development of facile drug delivery platform of ranibizumab fabricated PLGA-PEGylated magnetic nanoparticles for age-related macular degeneration therapy. J Photochem Photobiol B Biol 2018;183:133–6. https://doi.org/10.1016/j.jphotobiol.2018.04.033.
[36] Bourges JL, Gautier SE, Delie F, Bejjani RA, Jeanny JC, Gurny R, et al. Ocular drug delivery targeting the retina and retinal pigment epithelium using polylactide nanoparticles. Investig Ophthalmol Vis Sci 2003;44:3562–9. https://doi.org/10.1167/iovs.02-1068.
[37] Kim H, Csaky KG. Nanoparticle-integrin antagonist C16Y peptide treatment of choroidal neovascularization in rats. J Contr Release 2010;142:286–93. https://doi.org/10.1016/j.jconrel.2009.10.031.
[38] Wang YF, Liu CH, Ji TJ, Mehta M, Wang WP, Marino E, et al. Intravenous treatment of choroidal neovascularization by photo-targeted nanoparticles. Nat Commun 2019;10:804. https://doi.org/10.1038/s41467-019-08690-4.
[39] Seyfoddin A, Shaw J, Al-Kassas R. Solid lipid nanoparticles for ocular drug delivery. Drug Deliv 2010;17:467–89. https://doi.org/10.3109/10717544.2010.483257.
[40] Singh KH, Shinde UA. Development and evaluation of novel polymeric nanoparticles of brimonidine tartrate. Curr Drug Deliv 2010;7:244–51. https://doi.org/10.2174/156720110791561008.
[41] Gote V, Ansong M, Pal D. Prodrugs and nanomicelles to overcome ocular barriers for drug penetration. Expet Opin Drug Metabol Toxicol 2020;16: 885–906.
[42] Mandal A, Gote V, Pal D, Ogundele A, Mitra AK. Ocular pharmacokinetics of a topical ophthalmic nanomicellar solution of cyclosporine (Cequa(R)) for dry eye disease. Pharm Res (N Y) 2019;36:1–21.
[43] Mandal A, Cholkar K, Khurana V, Shah A, Agrahari V, Bisht R, et al. Topical formulation of self-assembled antiviral prodrug nanomicelles for targeted retinal delivery. Mol Pharm 2017;14:2056–69.
[44] Vaishya RD, Gokulgandhi M, Patel S, Minocha M, Mitra AK. Novel dexamethasone-loaded nanomicelles for the intermediate and posterior segment uveitis. AAPS PharmSciTech 2014;15:1238–51. https://doi.org/10.1208/s12249-014-0100-4.
[45] Ma FY, Nan KH, Lee S, Beadle JR, Hou HY, Freeman WR, et al. Micelle formulation of hexadecyloxypropyl-cidofovir (HDP-CDV) as an intravitreal long-lasting delivery system. Eur J Pharm Biopharm 2015;89:271–9. https://doi.org/10.1016/j.ejpb.2014.12.010.
[46] Alshamrani M, Sikder S, Coulibaly F, Mandal A, Pal D, Mitra AK. Self-assembling topical nanomicellar formulation to improve curcumin absorption across ocular tissues. AAPS PharmSciTech 2019;20:254. https://doi.org/10.1208/s12249-019-1404-1.
[47] Gote V, Mandal A, Alshamrani M, Pal D. Self-assembling tacrolimus nanomicelles for retinal drug delivery. Pharmaceutics 2020;12:1072. https://doi.org/10.3390/pharmaceutics12111072.
[48] Vaishya RD, Khurana V, Patel S, Mitra AK. Controlled ocular drug delivery with nanomicelles. Wiley Interdiscip Rev Nanomed Nanobiotechnol 2014;6: 422–37. https://doi.org/10.1002/wnan.1272.
[49] Song Z, Feng R, Sun M, Guo C, Gao Y, Li L, et al. Curcumin-loaded PLGA-PEG-PLGA triblock copolymeric micelles: preparation, pharmacokinetics and distribution *in vivo*. J Colloid Interface Sci 2011;354(1):116–23. https://doi.org/10.1016/j.jcis.2010.10.024.
[50] Qindeel M, Ahmed N, Shah KU, Ullah N. New, environment friendly approach for synthesis of amphiphilic PCL–PEG–PCL triblock copolymer: an efficient carrier for fabrication of nanomicelles. J Polym Environ 2020;28:1237–51. https://doi.org/10.1007/s10924-020-01683-1.
[51] Raza K, Kumar N, Misra C, Kaushik L, Guru SK, Kumar P, et al. Dextran-PLGA-loaded docetaxel micelles with enhanced cytotoxicity and better pharmacokinetic profile. Int J Biol Macromol 2016;88:206–12. https://doi.org/10.1016/j.ijbiomac.2016.03.064.

[52] Cholkar K, Hariharan S, Gunda S, Mitra AK. Optimization of dexamethasone mixed nanomicellar formulation. AAPS PharmSciTech 2014;15:1454–67. https://doi.org/10.1208/s12249-014-0159-y.
[53] Bilati U, Allémann E, Doelker E. Development of a nanoprecipitation method intended for the entrapment of hydrophilic drugs into nanoparticles. Eur J Pharmaceut Sci 2005;24(1):67–75. https://doi.org/10.1016/j.ejps.2004.09.011.
[54] Kohler N, Sun C, Wang J, Zhang M. Methotrexate-modified superparamagnetic nanoparticles and their intracellular uptake into human cancer cells. Langmuir 2005;21(19):8858–64. https://doi.org/10.1021/la0503451.
[55] Yang X, Hong H, Grailer JJ, Rowland IJ, Javadi A, Hurley SA, et al. cRGD-functionalized, DOX-conjugated, and 64Cu-labeled superparamagnetic iron oxide nanoparticles for targeted anticancer drug delivery and PET/MR imaging. Biomaterials 2011;32(17):4151–60. https://doi.org/10.1016/j.biomaterials.2011.02.006.
[56] Pramanik A, Laha D, Pramanik A, Chattopadhyay S, Dash SK, Roy S, et al. An in-vivo study for targeted delivery of copper-organiccomplex to breast cancer using chitosan polymer nanoparticles. Mater Sci Eng C 2016;65:327–37. https://doi.org/10.1016/j.msec.2016.05.014.
[57] Laha D, Pramanik A, Chattopadhyay S, Dash SK, Roy S, Pramanik P, et al. Folic acid modified copper oxide nanoparticles for targeted delivery in *in vitro* and *in vivo* systems. RSC Adv 2015;5:68169–78. https://doi.org/10.1039/C5RA08110F.
[58] Lu Y, Yue Z, Xie J, Wang W, Zhu H, Zhang E, et al. Micelles with ultralow critical micelle concentration as carriers for drug delivery. Nat Biomed Eng 2018;2:318–25. https://doi.org/10.1038/s41551-018-0234-x.
[59] Shen J, Lu GW, Hughes P. Targeted ocular drug delivery with pharmacokinetic/pharmacodynamic considerations. Pharm Res (N Y) 2018;35:217. https://doi.org/10.1007/s11095-018-2498-y.
[60] Cholkar K, Gunda S, Earla R, Pal D, Mitra AK. Nanomicellar topical aqueous drop formulation of rapamycin for back-of-the-eye delivery. AAPS PharmSciTech 2015;16:610–22. https://doi.org/10.1208/s12249-014-0244-2.
[61] Guo C, Zhang Y, Yang Z, Li M, Li F, Cui F, et al. Nanomicelle formulation for topical delivery of cyclosporine A into the cornea: *in vitro* mechanism and *in vivo* permeation evaluation. Sci Rep 2015;5:12968. https://doi.org/10.1038/srep12968.
[62] Mehra N, Aqil M, Sultana Y. A grafted copolymer-based nanomicelles for topical ocular delivery of everolimus: formulation, characterization, ex-vivo permeation, in-vitro ocular toxicity, and stability study. Eur J Pharmaceut Sci 2021;159:105735. https://doi.org/10.1016/j.ejps.2021.105735.
[63] Oremusová J, Vitková Z, Vitko A, Tárník M, Miklovičová E, Ivánková O, et al. Effect of molecular composition of head group and temperature on micellar properties of ionic surfactants with C12 alkyl chain. Molecules 2019;24:651. https://doi.org/10.3390/molecules24030651.
[64] Hwang MJ, Suh JM, Bae YH, Kim SW, Jeong B. Caprolactonic poloxamer analog: pEG-PCL-PEG. Biomacromolecules 2005;2:885–90. https://doi.org/10.1021/bm049347a.
[65] Alami-Milani M, Zakeri-Milani P, Valizadeh H, Salehi R, Jelvehgari M. Preparation and evaluation of PCL-PEG-PCL micelles as potential nanocarriers for ocular delivery of dexamethasone. Iran J Basic Med Sci 2018;2:153. https://doi.org/10.22038/IJBMS.2017.26590.6513.
[66] Brandt JV, Piazza RD, dos Santos CC, Vega-Chacon J, Amantea BE, Pinto GC, et al. Synthesis and colloidal characterization of folic acid-modified PEG-b-PCL Micelles for methotrexate delivery. Colloids Surf, B 2019;6:228–34. https://doi.org/10.1016/j.colsurfb.2019.02.008.
[67] Dong P, Wang X, Gu Y, Wang Y, Wang Y, Gong C, et al. Self-assembled biodegradable micelles based on star-shaped PCL-b-PEG copolymers for chemotherapeutic drug delivery. Colloids Surf, A 2010;1–3:128–34. https://doi.org/10.1016/j.colsurfa.2010.01.037.
[68] Li Z, Liu M, Ke L, Wang LJ, Wu C, Li C, et al. Flexible polymeric nanosized micelles for ophthalmic drug delivery: research progress in the last three years. Nanoscale Adv 2021;3(18):5240–54. https://doi.org/10.1039/D1NA00596K.
[69] Cai R, Zhang L, Chi H. Recent development of polymer nanomicelles in the treatment of eye diseases. Front Bioeng Biotechnol 2023;11. https://doi.org/10.3389/fbioe.2023.1246974.
[70] Lu P, Liang Z, Zhang Z, Yang J, Song F, Zhou T, et al. Novel nanomicelle butenafine formulation for ocular drug delivery against fungal keratitis: *in vitro* and *in vivo* study. Eur J Pharmaceut Sci 2024;192:106629. https://doi.org/10.1016/j.ejps.2023.106629.
[71] Chen Y, Chen H, Zeng D, Tian Y, Chen F, Feng J, et al. Core/shell structured hollow mesoporous nanocapsules: a potential platform for simultaneous cell imaging and anticancer drug delivery. ACS Nano 2010;4:6001. https://doi.org/10.1021/nn1015117.
[72] Nagarwal RC, Kumar R, Dhanawat M, Pandit J. Modified PLA nano in situ gel: a potential ophthalmic drug delivery system. Colloids Surf B 2011;86:28. https://doi.org/10.1016/j.colsurfb.2011.03.023.
[73] Trinh HM, Cholkar K, Joseph M, Yang X, Mitra AK. Clear, aqueous topical drop of triamcinolone acetonide. AAPS PharmSciTech 2017;18:2466–78. https://doi.org/10.1208/s12249-017-0714-4.
[74] Cholkar K, Gilger BC, Mitra AK. Topical, aqueous, clear cyclosporine formulation design for anterior and posterior ocular delivery. Transl Vis Sci Technol 2015;4. https://doi.org/10.1167/tvst.4.3.1.
[75] Manjili HK, Malvandi H, Mousavi MS, Attari E, Danafar H. *In vitro* and *in vivo* delivery of artemisinin loaded PCL–PEG–PCL micelles and its pharmacokinetic study. Artif Cells, Nanomed Biotechnol 2018;46(5):926–36. https://doi.org/10.1080/21691401.2017.1347880.
[76] Ashwanikumar N, Kumar NA, Nair SA, Kumar GV. Dual drug delivery of 5-fluorouracil (5-FU) and methotrexate (MTX) through random copolymeric nanomicelles of PLGA and polyethylenimine demonstrating enhanced cell uptake and cytotoxicity. Colloids Surf B 2014;122:520–8. https://doi.org/10.1016/j.colsurfb.2014.07.024.
[77] Caldorera-Moore ME, Liechty WB, Peppas NA. Responsive theranostic systems: integration of diagnostic imaging agents and responsive controlled release drug delivery carriers. Acc Chem Res 2011;44(10):1061–70. https://doi.org/10.1021/ar2001777.
[78] Ahn SM, Ahn J, Cha S, Yun C, Park TK, Kim YJ, et al. Morphologic and electrophysiologic findings of retinal degeneration after intravitreal sodium iodate injection following vitrectomy in canines. Sci Rep 2020;10:3588. https://doi.org/10.1038/s41598-020-60579-1.
[79] Yang Y, Ng TK, Ye C, Yip YW, Law K, Chan SO, et al. Assessing sodium iodate-induced outer retinal changes in rats using confocal scanning laser ophthalmoscopy and optical coherence tomography. Invest Ophthalmol Vis Sci 2014;55:696–705. https://doi.org/10.1167/iovs.13-12477.
[80] Hanus J, Anderson C, Sarraf D, Ma J, Wang S. Retinal pigment epithelial cell necroptosis in response to sodium iodate. Cell Death Dis 2016;2:16054. https://doi.org/10.1038/cddiscovery.2016.54.